0.1 Rapid Compression Machine

0.1.1 Experimental Procedure

The studies in this dissertation were conducted using the Rapid Compression Machine (RCM) constructed by Mittal around 2005 and described in the work of Mittal and Sung [1] and Mittal [2]. This RCM has been used to study the autoignition behavior of a number of fuels, including *n*-decane, methylcyclohexane, hydrogen, syngas, dimethyl ether, methanol, toluene, benzene, di-isobutylene, iso-octane, jet fuel, and gasoline [3–18], in addition to the studies presented in this work.

A modern RCM operates by rapidly compressing (hence the name) a test gas mixture to targeted pressure and temperature conditions. The compression is effected by either a single piston or dual, opposed pistons. Upon reaching the targeted state, the piston (or pistons) is stopped and fixed in place so that the reactions proceed in a constant volume reactor. When studying autoignition with an RCM, the primary data are the measured pressure traces during and after the compression stroke. These pressure traces are processed to derive information such as the pressure and temperature at the end of compression (EOC) and the ignition delay. It is also possible to employ laser diagnostics or extract gas samples from the reactor to examine reaction pathways in more detail.

The present RCM is a pneumatically-driven/hydraulically-stopped single-piston arrangement. A schematic of the RCM is shown in Fig. 1 and an image is shown in Fig. 2. The RCM consists of four chambers and three pistons that are used to control the machine. The chambers are called the reaction chamber, the hydraulic chamber, the pneumatic chamber, and the driving tank; similarly, the pistons are called the reactor, hydraulic, and pneumatic pistons and are each installed in the chamber of the same name. The rear of the reaction chamber is bolted to the front of the hydraulic chamber; seals in the face of the hydraulic chamber prevent oil from leaking into and contaminating the reaction chamber. The driving tank and the rear of the pneumatic chamber are connected by a union; a seal around the circumference of the pneumatic piston seals gas in the driving tank from the front of the pneumatic chamber. Thus, the pneumatic piston can be driven by pressure from the

driving tank on its rear and pressure from the pneumatic chamber on its front. The three pistons are connected by a rod running from the front of the pneumatic piston to the rear of the reactor piston so that they move as one; this will be referred to as the piston assembly.

At the start of an experimental run, with the piston in the EOC position, the reaction chamber is vacuumed to less than 1 Torr. Next, the piston assembly is retracted by pressurizing the front face of the piston in the pneumatic chamber. For safety, and to prevent damage to the RCM, the driving tank should be filled to limit the acceleration of the piston assembly during the retraction. The pressure on the front of the pneumatic piston pulls the piston assembly rearward and seats the rear of the hydraulic piston onto an O-ring in the rear of the hydraulic chamber. The hydraulic chamber is filled with oil to a pressure of approximately 800 psi, providing a rearward force on the front face of the hydraulic piston. Then, the air pressure is released from the front of the pneumatic chamber and the driving tank is filled to the desired driving pressure. The force on the hydraulic piston opposes the force on the pneumatic piston from the driving tank and the piston assembly remains at rest. Then, the reaction chamber is filled with the required initial pressure of test gas mixture from the mixing tank. Finally, compression is triggered by releasing the hydraulic pressure through an electrically-operated solenoid valve. The piston assembly is driven forward by the unbalanced force from the pressure in the driving tank on the pneumatic piston. The gases in the reaction chamber are brought to the compressed pressure (P_C) and compressed temperature (T_C) conditions in approximately 30–50 ms.

The required driving pressure for a given EOC pressure can be estimated from a force balance between the force on the pneumatic piston from the driving tank and the force on the reactor piston from the test gases, as shown in Eq. (1c).

$$P_{d,\min} \cdot A_p = P_{r,\text{EOC}} \cdot A_r \tag{1a}$$

$$P_{d,\min} \cdot \frac{\pi d_p^2}{4} = P_{r,\text{EOC}} \cdot \frac{\pi d_r^2}{4} \tag{1b}$$

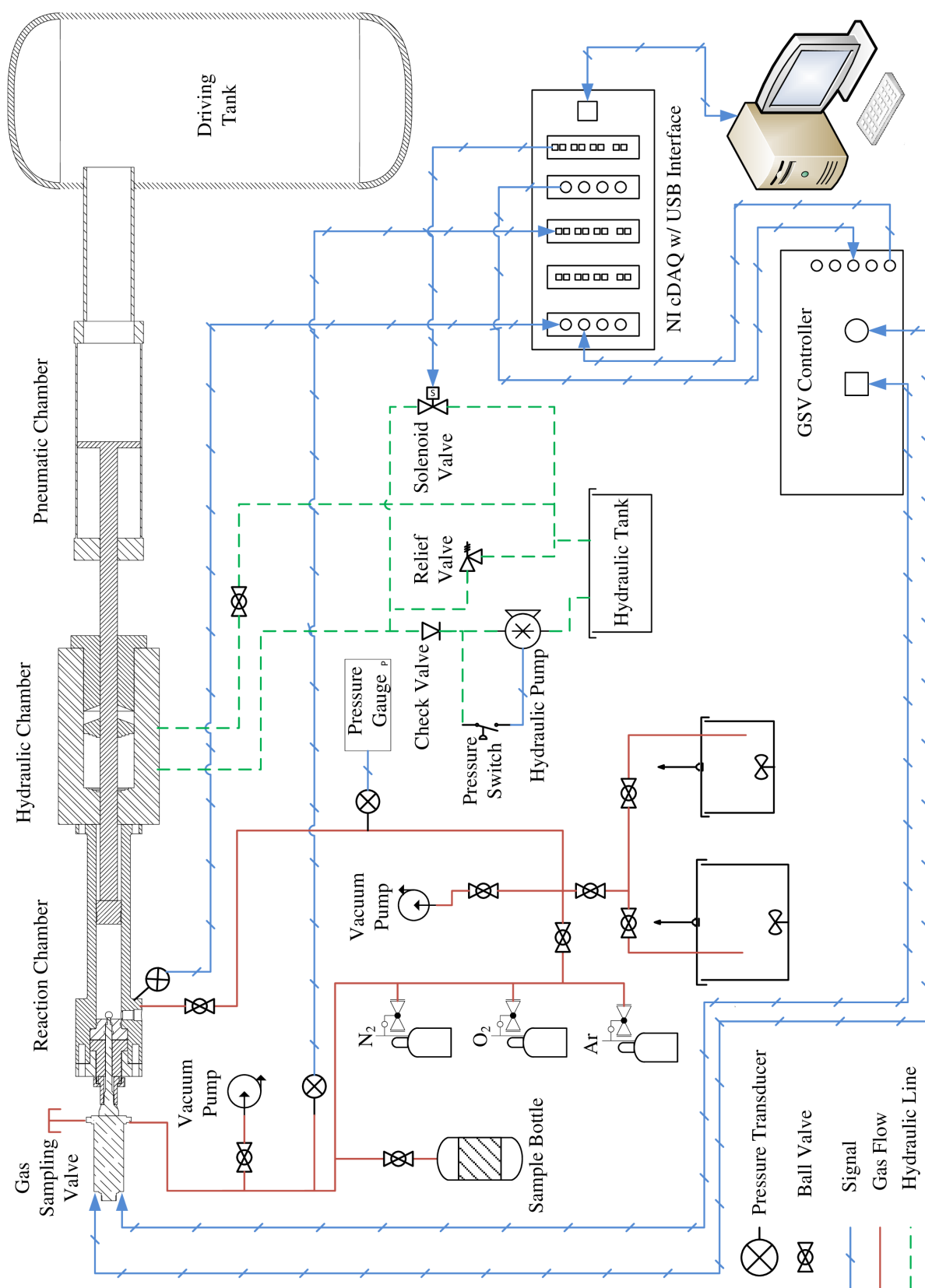$$P_{d,\min} = P_{r,\text{EOC}} \cdot \frac{d_r^2}{d_p^2} \tag{1c}$$

2

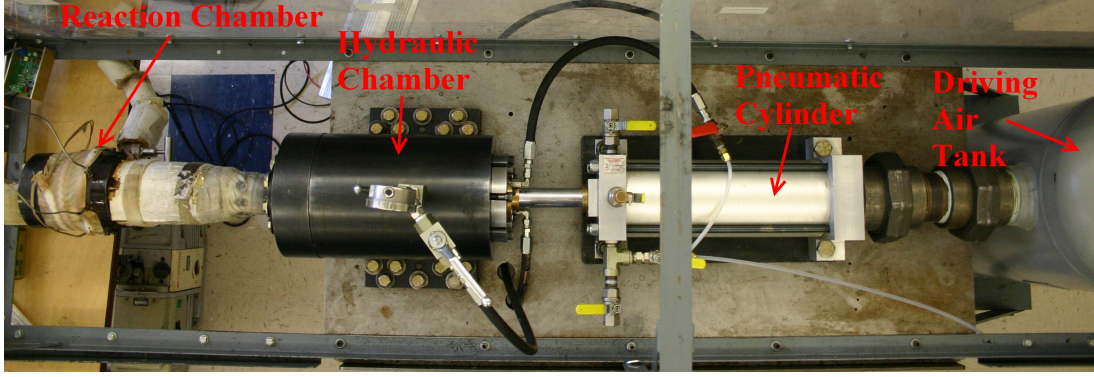**Figure 1**: Schematic of the RCM. Not to scale

Figure 2: Photograph of the RCM.

In Eq. (1), $P_{d,min}$ is the minimum driving pressure, A_p is the cross-sectional area of the pneumatic piston, $P_{r,EOC}$ is the pressure in the reactor at the EOC (i.e. P_C), A_r is the cross-sectional area of the reactor piston, d_p is the diameter of the pneumatic piston, and d_r is the diameter of the reactor piston.

The minimum driving pressure is such that the piston does not rebound at the EOC due to pressure on the reactor piston. So that the driving pressure can be much lower than the EOC pressure, the diameter ratio of the reactor piston to the driver piston is 2/5, allowing a factor of 6.25 lower driving pressure than EOC pressure. The actual driving pressure should exceed the minimum by some safety margin so that the reactor remains at constant volume even if there is some pressure rise due to heat release in the reaction chamber prior to the main ignition.

There is not a theoretical upper limit on the driving pressure. It is desired that the piston should reach the EOC conditions in as short a time as possible to minimize heat loss from the reactants to the reactor walls and minimize the time for reactions to occur during the compression stroke. This implies that the driving pressure should be made as high as possible so that the highest piston velocity is achieved. However, higher piston velocities require a higher deceleration at the EOC. In the present RCM, the deceleration is provided by venting the hydraulic oil between steps on the hydraulic piston and matched steps on the front of the hydraulic chamber. If the piston is overdriven—that is, the driving pressure is too high—the piston will not be sufficiently decelerated by the oil venting and will impact the front of the hydraulic chamber at high velocity. This can

4

damage the RCM and cause the piston to rebound elastically. It also generates substantial noise in the pressure trace and should be avoided.

Typical driving gas pressures are between 50 psi for $P_C = 15$ bar experiments to 125 psi for $P_C = 50$ bar experiments. These driving pressures represent a good compromise between the minimum required for no rebound at EOC due to pressure and no rebound at EOC due to elastic reaction. Nonetheless, a small amount of piston rebound can be expected during/after the main ignition event. This small rebound may have an effect on the computation of ignition delay if it reduces the pressure rise rate during the ignition; it is expected that this effect will be very small relative to the typical random uncertainty in ignition delay experiments. Moreover, the driving pressures required to balance the full pressure rise during to ignition are more likely cause elastic rebound, especially for high P_C when the post-ignition pressure rise is greater.

The EOC conditions (P_C and T_C) can be independently varied. This is made possible by independent variation of the compression ratio, initial pressure and initial temperature, and the specific heat ratio of the test gases. The compression ratio can be increased by adding spacers onto the rear of the hydraulic chamber, increasing the stroke, and can be reduced by adding split shims onto the rear of the reaction chamber, increasing the EOC clearance length. Adjustment of the specific heat ratio of the gas can be accomplished by substituting components (i.e. substituting Ar for N_2 results in higher P_C and T_C if all other conditions are fixed). The initial temperature is controlled by heaters, as described in the following section.

0.1.2   Test Gas Mixture Preparation

Fuel/oxidizer pre-mixtures are prepared in two mixing tanks, one approximately 17 L and the other approximately 15 L in volume. These large volumes allow many runs to be conducted from one mixture preparation. The mixing tanks are connected to the reaction chamber by flexible stainless steel manifold tubing. The tanks, reaction chamber, and connecting manifold are wrapped in heating tape and insulation to control the initial temperature of the mixture. Temperature controllers from Omega Engineering use thermocouples placed on the lid of each mixing tank, approximately

in the center of each mixing tank, embedded in the wall of the reaction chamber, and near the inlet valve of the reaction chamber to control the preheat temperature of the mixture. A static pressure transducer measures the pressure in the manifold and mixing tanks. This transducer is used during mixture preparation and to measure the initial pressure of a given experiment. Two transducers are for various experiments in this work, as described below in Sec. 0.1.7.2.

Most of the fuels studied in this work are liquids at room temperature and pressure and have relatively low vapor pressure. A similar procedure, outlined below, was used for all of the butanol isomers, *iso*-pentanol, and methylcyclohexane; specific procedures are given in the chapter relevant to each fuel. First, the mixing tanks are vacuumed to an ultimate pressure less than 5 Torr. The liquid fuel is massed in a syringe to a precision of 0.01 g prior to injection through a septum. Proportions of O_2, N_2, and Ar are added manometrically at room temperature. The preheat temperature of the RCM is set above the saturation point for each fuel to ensure complete vaporization. The vapor pressure as a function of temperature is calculated according to fits taken from Yaws [19]. A magnetic stirrer mixes the reactants. The temperature inside the mixing tank is allowed to equilibrate for approximately 1.5 h.

This approach to mixture preparation has been validated in several previous studies by withdrawing gas samples from the mixing tank and analyzing the contents by GC/MS [20], GC-FID [3], and GC-TCD [7]. These studies have verified the concentration of *n*-butanol, *n*-decane, and water, respectively. In addition, both the work by Kumar et al. [3] on *n*-decane and the study of Weber et al. [20] on *n*-butanol confirmed that there was no fuel decomposition over the course of a typical set of experiments. Furthermore, within this study, each new mixture preparation is checked against previously tested conditions to ensure reproducibility.

0.1.3 Definition of Ignition Delay

The pressure in the reaction chamber during an experiment is monitored by a Kistler 6125B piezo-electric dynamic pressure transducer. The charge signal from the transducer is amplified and converted to a voltage by a Kistler 5010B charge amplifier. The voltage is sent to a National Instruments
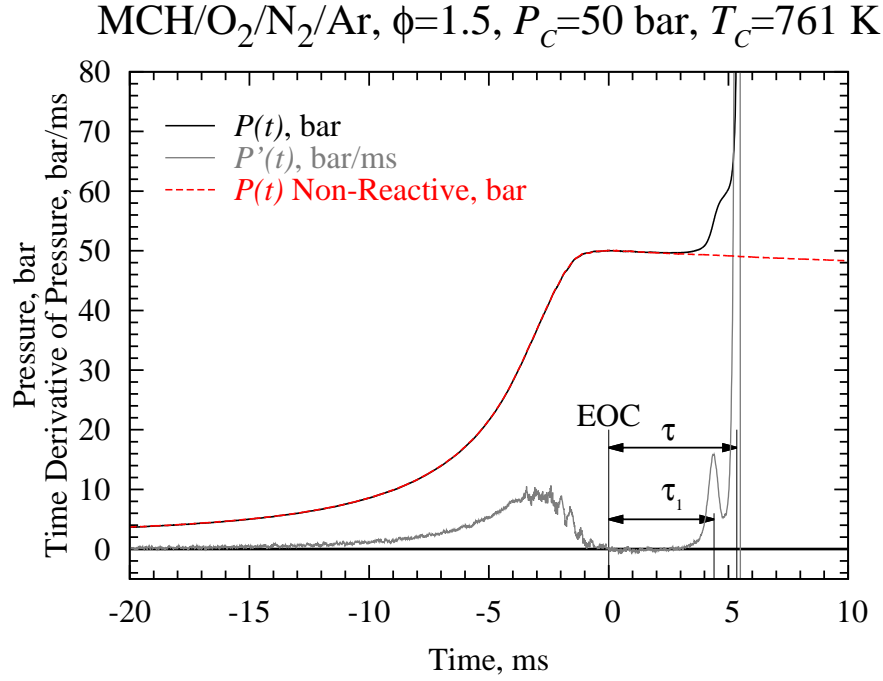
Figure 3: Representative pressure trace indicating the definition of the first stage and overall ignition delays and the corresponding non-reactive pressure trace. EOC stands for End of Compression.

cDAQ equipped with the NI-9215 module. The signal is recorded by a LabView VirtualInstrument at 50 kHz.

Figure 3 shows a representative pressure trace from these experiments with methylcyclohexane (MCH) at $P_C = 50$ bar, $T_C = 761$ K, and $\phi = 1.5$ (See **??**). Note that Fig. 3 shows a case with two stages of ignition; not all of the fuels studied had conditions that showed two-stage ignition. Nonetheless, the ignition delay is consistently defined in all the work in this study. The definitions of the EOC and the ignition delays are indicated on the figure. The end of compression time is defined as the time when the pressure reaches its maximum before first stage ignition occurs, or for cases where there is no first stage ignition, the maximum pressure before the overall ignition occurs. The first stage ignition delay is the time from the end of compression until the first peak in the time derivative of the pressure. The overall ignition delay is the time from the end of compression until the largest peak in the time derivative of the pressure.

Each unique P_C and T_C condition is repeated at least 5 times to ensure repeatability of the experiments. The experiment closest to the mean of the runs at a particular condition is chosen for

analysis and presentation. The standard deviation of all of the runs at a condition is less than 10% of the mean in all cases.

0.1.4   Non-Reactive Experiments

Figure 3 also shows a non-reactive pressure trace. Due to heat loss from the test mixture to the cold reactor walls, the pressure and temperature of the gas in the reaction chamber will decrease after the end of compression. A non-reactive pressure trace is measured that corresponds to each unique P_C and T_C condition studied to quantify the effect of the heat loss on the ignition process and to verify that no heat release has occurred during the compression stroke. The non-reactive pressure trace is acquired by replacing the oxygen in the oxidizer with nitrogen, so that the specific heat ratio of the initial mixture is maintained, but the heat release due to exothermic oxidation reactions is eliminated. Maintaining a similar specific heat ratio ensures that the non-reactive experiment faithfully reproduces the conditions of the reactive experiment. A representative non-reactive pressure trace is shown in Fig. 3 corresponding to the experimental conditions in the figure.

0.1.5   Reaction Chamber Homogeneity

An RCM to be used for studies of homogeneous chemistry—as in this study—must ensure that homogeneous conditions exist inside the reaction chamber for the duration of the experiment. Due to the high piston velocities required to minimize heat loss and reaction during the compression stroke, complex fluid mechanical effects can strongly affect the state of the reactants at the EOC. The most important of these effects is caused by the motion of the piston itself, where the piston pushes the wall boundary layer into a roll-up vortex [21]. This cold vortex mixes with the hotter gases near the center of the reaction chamber and causes large spatial inhomogeneities of temperature and species.

To facilitate spatially homogeneous conditions in the reactor and reduce the effect of the roll-up vortex, it is necessary to trap the boundary layer. This is accomplished on the present RCM by a

crevice machined into the crown of the piston, shown in cross-section in Fig. 4. The boundary layer enters the crevice through the converging section as the piston moves forward and is trapped within the crevice. The dimensions of the crevice were optimized by Mittal [2] through CFD simulations. Subsequently, Mittal and Sung [22] experimentally showed that the optimized crevice design provides homogeneous conditions in the reaction chamber up to approximately 150 ms after the EOC. By using PLIF measurements of acetone-seeded mixtures, Mittal and Sung [22] showed that there was a core region of gases near the center of the reactor whose temperature remained spatially homogeneous.
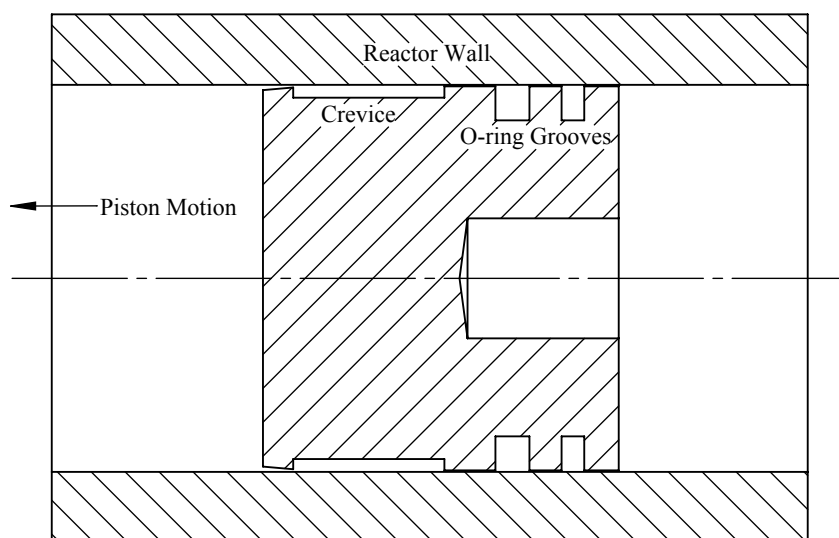

Figure 4: Creviced piston installed in the present RCM.

0.1.6 Determination of Reactant Temperature

In general, it is rather difficult to directly measure the temperature of the gases in the reaction chamber during and after compression. Intrusive methods such as thermocouples may introduce inhomogeneities into the reaction chamber and non-intrusive optical techniques are difficult to set up and require extensive calibration at the pressures of interest in RCM studies. Thus, the temper-

ature is determined indirectly by applying an assumption called the "adiabatic core hypothesis" to the reaction chamber [1, 21].

If all of the gases in the reaction chamber were compressed isentropically, the temperature at the end of compression could be found by the following relations:

$$\ln(\text{CR}) = \int_{T_0}^{T_{ic}} \frac{1}{T(\gamma - 1)} \, dT \tag{2a}$$

$$\ln\left(\frac{P_{ic}}{P_0}\right) = \int_{T_0}^{T_{ic}} \frac{\gamma}{T(\gamma - 1)} \, dT \tag{2b}$$

where CR is the volumetric compression ratio, T_0 is the initial temperature, T_{ic} is the temperature at the end of isentropic compression, γ is the temperature-dependent ratio of specific heats, P_{ic} is the pressure at the end of isentropic compression, and P_0 is the initial pressure.

However, experiments show that the measured pressure in the reaction chamber does not reach the value of P_{ic} calculated by using the geometric compression ratio. The difference is due to finite heat loss from the reactants to the reactor walls and the crevice volume during the compression. Under the adiabatic core hypothesis, it is assumed that the heat loss from the reactants only occurs in a thin boundary layer near the wall, and the central core region is unaffected by heat loss (i.e. the core is adiabatic) [23]. Thus, the heat loss is modeled as an effective reduction in the compression ratio, and the temperature during the compression stroke can be calculated by:

$$\ln\left(\frac{P_C}{P_0}\right) = \int_{T_0}^{T_C} \frac{\gamma}{T(\gamma - 1)} \, dT \tag{3}$$

where P_C is the measured pressure at the end of compression, T_C is the temperature at the end of compression, and the other variables are the same as in Eq. (2).

After the end of compression, the pressure in the reaction chamber decreases, as can be seen in Fig. 3. This pressure decrease is caused by heat loss from the reactants in the constant volume reaction chamber and is accompanied by a decrease in the temperature of the reactants. To model the thermodynamic state after the end of compression, the adiabatic core hypothesis is applied and

the heat loss is assumed to occur only in a thin boundary layer near the reactor walls. Thus, the core region is modeled as adiabatic, and the heat loss from the boundary layer is be modeled as an isentropic volume expansion.

In general, the specific heat ratio used in Eqs. (2) and (3) is an unknown function of temperature and composition, so Eq. (3) cannot be integrated directly to find T_C. If the specific heats are parameterized with a linear fit and the composition is assumed to be fixed, it is possible to integrate Eq. (3) directly, but this process is quite tedious; nonetheless, it will be applied in Sec. 0.1.7 to determine the uncertainty of T_C. In general, the simplest method of calculating T_C is to use software to numerically integrate Eq. (3).

In this work, the CHEMKIN-Pro [24] software is used to perform the numerical integration and calculation of T_C. The CHEMKIN-Pro software provides the facility for a user-specified volume as a function of time to be applied to a homogeneous, adiabatic reactor. Since the adiabatic core of the reaction chamber is modeled as undergoing an isentropic volumetric compression followed by an isentropic volumetric expansion, the user-specified volume functionality is used to compute the RCM reactor state as a function of time. A volume trace for simulation is computed from the measured pressure trace using the isentropic relation:

$$\frac{V_2}{V_1} = \left[\frac{P_1}{P_2}\right]^{\frac{1}{\gamma}} \tag{4}$$

where V_1 and V_2 are the volumes at consecutive time points, P_1 and P_2 are the pressures at consecutive time points, and γ is the temperature dependent specific heat. This equation is applied during and after the compression stroke to calculate the volume trace. Since the non-reactive experiment requires slightly different initial pressure (on the order of 5 torr) to reach the same compressed pressure as the reactive experiment—due to the slightly different specific heat ratio in the non-reactive experiment as compared to the reactive experiment—the reactive pressure trace is used to compute the volume trace until EOC; after EOC, the corresponding non-reactive pressure trace is used. In Eq. (4) it is assumed that changes in composition of the reactants are negligible during the com-

pression stroke, which is confirmed by comparing simulations with and without reaction steps in the chemical kinetic model. The EOC conditions are the same in both cases. The initial volume is arbitrarily taken to be equal to 1.

For use in Eq. (4), the temperature-dependent specific heat ratio γ is tabulated for each time point. Thus, the temperature at each time point must also be computed by using the isentropic relation for temperature:

$$\frac{T_2}{T_1} = \left[\frac{P_2}{P_1}\right]^{\frac{\gamma-1}{\gamma}}$$

(5)

where T_2 and T_1 are the temperatures at consecutive time points. Since T_2 depends on the value of γ, which in turn depends on T_2, Eq. (5) is iterated until the temperature changes by less than one tenth of one percent on consecutive iterations. Once again, it is assumed that changes in composition have a negligible influence on the ratio of specific heats. The temperature calculated by Eq. (5) is typically within 1K of the temperature calculated by CHEMKIN-Pro.

0.1.7   Uncertainty of Ignition Delay and Compressed Temperature

The uncertainty of the compressed temperature is an important parameter to report. Since T_C is not measured, we must perform an uncertainty propagation analysis on the equation used to calculate T_C, Eq. (3). First, we simplify the term involving γ in Eq. (3). By definition, γ is the ratio of the specific heat at constant pressure to that at constant volume

$$\gamma \equiv \frac{C_p}{C_v} = \frac{C_p/R}{C_v/R} = \frac{\hat{C}_p}{\hat{C}_v}$$

(6)

where C_p and C_v are the specific heats in molar units at constant pressure and volume, respectively, and R is the universal gas constant, used to produce non-dimensional specific heats, indicated by a hat. The difference between the non-dimensional specific heats is one, $\hat{C}_v = \hat{C}_p - 1$. Then, it

12

follows that

$$\frac{\gamma}{\gamma-1} = \frac{\frac{\hat{C}_p}{\hat{C}_v}}{\frac{\hat{C}_p}{\hat{C}_v}-1} = \frac{\frac{\hat{C}_p}{\hat{C}_p-1}}{\frac{\hat{C}_p}{\hat{C}_p-1}-1} = \frac{\frac{\hat{C}_p}{\hat{C}_p-1}}{\frac{1}{\hat{C}_p-1}} = \hat{C}_p \tag{7}$$

In Eq. (3), the total specific heat ratio for the mixture should be used; thus, the simplification as shown in Eq. (7) requires that the specific heat $\hat{C}_p$ also be the total specific heat. In the following, we assume that there is negligible change of the total specific heat due to changes in reactant mole fractions, as for Eqs. (4) and (5). The total specific heat is simply the sum of the product of the species mole fractions and their specific heats

$$C_{p,\text{total}} = \sum_i X_i C_{p,i} \tag{8a}$$

$$\hat{C}_{p,\text{total}} = \frac{\sum_i X_i C_{p,i}}{R} \tag{8b}$$

where i indicates the species and X_i is the species mole fraction. In the NASA polynomial formulation used by CHEMKIN, the non-dimensional specific heat at constant pressure as a function of temperature is represented by a fourth-order polynomial fit

$$\hat{C}_{p,i} = c_{1,i} + c_{2,i}T + c_{3,i}T^2 + c_{4,i}T^3 + c_{5,i}T^4 \tag{9}$$

In general, this means that the specific heat can be non-linear. However, since the mixtures prepared in this study are composed primarily of O_2, N_2 and Ar (i.e. no more than 7% of any mixture is the fuel), and since the specific heats of O_2, N_2 and Ar are only weakly temperature dependent over the range of temperatures experienced during compression, for the purposes of this uncertainty

13

analysis, we will approximate the total specific heat as a linear function of temperature:

$$\hat{C}_{p,\text{total}} = \sum_i X_i \hat{C}_{p,i}$$

$$= \sum_i X_i \left(\sum_{j=1}^{5} c_{j,i} T^{j-1} \right) \tag{10}$$

$$\approx a + bT$$

a and b are found by fitting the total non-dimensional specific heat over the temperature range from 300–1100 K, as discussed below in Sec. 0.1.7.4.

With this approximation of the specific heat, we can integrate Eq. (3) to find the compressed temperature

$$\ln \frac{P_C}{P_0} = \int_{T_0}^{T_C} \frac{\gamma}{T(\gamma - 1)} \, dT \tag{11a}$$

$$= \int_{T_0}^{T_C} \frac{\hat{C}_p}{T} \, dT \tag{11b}$$

$$= \int_{T_0}^{T_C} \frac{a + bT}{T} \, dT \tag{11c}$$

$$= \left[a \ln T + bT \right]_{T_0}^{T_C} \tag{11d}$$

$$\ln \frac{P_C}{P_0} + (a \ln T_0 + bT_0) = a \ln T_C + bT_C \tag{11e}$$

Equation (11e) can be solved explicitly for T_C by using Lambert's W function [25], but this function is somewhat complex. Instead, Eq. (11e) is simplified by performing a Taylor expansion of the right hand side and solving for T_C:

$$a \ln T_C + bT_C = a \ln T_e + bT_e + \left(\frac{a}{T_e} + b \right)(T_C - T_e) \tag{12}$$

$$T_C = \frac{\ln \frac{P_C}{P_0} + a \ln \frac{T_0}{T_e} + b(T_0 - T_e)}{\frac{a}{T_e} + b} + T_e \tag{13}$$

14

where T_e is the temperature about which the Taylor expansion is performed.

With an explicit function for T_C, we can estimate the uncertainty in T_C by the root square sum of the uncertainty in the parameters in Eq. (13) multiplied by the partial derivative of Eq. (13) with respect to each of the parameters [26]. The parameters are P_C, P_0, T_0, a, and b and are assumed to be independent.

$$U_{T_C} = \sqrt{\left(\frac{\partial T_C}{\partial P_C} U_{P_C}\right)^2 + \left(\frac{\partial T_C}{\partial P_0} U_{P_0}\right)^2 + \left(\frac{\partial T_C}{\partial T_0} U_{T_0}\right)^2 + \left(\frac{\partial T_C}{\partial a} U_a\right)^2 + \left(\frac{\partial T_C}{\partial b} U_b\right)^2} \quad (14)$$

The uncertainties of the parameters, U_j in Eq. (14), are in general found by their own root square sum procedure

$$U_j{}^2 = B_j{}^2 + R_j{}^2 \quad (15)$$

where the subscript j represents one of the parameters in Eq. (13). The total uncertainty of a particular parameter is composed of two parts, the systematic or bias uncertainty (B_j) and the precision or random uncertainty (R_j). In general, the bias uncertainty is contained in the measurement equipment and can be reduced, e.g. by using different equipment; the random uncertainty is inherent in any measured process and cannot be reduced by experimental techniques. The bias and precision uncertainties for each parameter will be discussed in the following.

0.1.7.1 Uncertainty in Initial Temperature

The bias uncertainty in the initial temperature is due to the standard limits of error of the K-type thermocouple used to measure the initial temperature. According to the Omega Engineering specifications, this is "the greater of 2.2 °C or 0.75%". The largest initial temperature used in this work, 413 K, leads to an uncertainty of ± 3 K; thus, $B_{T_O} = 3$ K. Bias uncertainty due to the A/D converter in the process meter is negligible compared to this uncertainty. The precision uncertainty is due to the limit of precision of the display on the Omega Engineering CNi3254 process meter used to

control the process temperature. This is ± 0.05 K. The total uncertainty of the initial temperature is

$$U_{T_0} = \sqrt{\left(B_{T_0}\right)^2 + \left(R_{T_0}\right)^2} = \sqrt{\left(3\,\text{K}\right)^2 + \left(0.05\,\text{K}\right)^2} = 3\,\text{K} \tag{16}$$

0.1.7.2 Uncertainty in Initial Pressure

The bias uncertainty in the initial pressure is due to the standard error in the pressure transducer used to measure the initial pressure. Two different pressure transducers have been used in this study; the first, an Omega Engineering PX-303 (range: 0–50 psia), has a full scale uncertainty of 1.25%, or ± 0.625 psi (4309.2 Pa). The second transducer is an Omega Engineering MMA100V10T2D0T4A6 type (range: 0–5200 Torr) and was purchased because preliminary results of this uncertainty analysis indicated that the largest contributor to the uncertainty of T_C was the initial pressure measurement. The full scale uncertainty of the MMA type transducers is 0.05%, resulting in an uncertainty of ± 2.6 Torr (346.6 Pa), an order of magnitude lower than the PX-303 while also providing more than double the operating range. Total uncertainties using the appropriate pressure transducer are reported in each experimental section of this work; both transducers will be analyzed in this section. Bias uncertainty due to the signal acquisition equipment is negligible compared to the standard error in the pressure transducers.

The precision uncertainty is due to the limit of precision of the display on the Omega Engineering DP41-B process meter used to monitor the initial pressure. This is ± 0.005 Torr (0.666 Pa). The total uncertainty of the initial pressure is

$$U_{P_0} = \sqrt{\left(B_{P_0}\right)^2 + \left(R_{P_0}\right)^2} = \sqrt{\left(4309.2\,\text{Pa}\right)^2 + \left(0.666\,\text{Pa}\right)^2} = 4309.2\,\text{Pa} \tag{17a}$$

$$U_{P_0} = \sqrt{\left(B_{P_0}\right)^2 + \left(R_{P_0}\right)^2} = \sqrt{\left(346.6\,\text{Pa}\right)^2 + \left(0.666\,\text{Pa}\right)^2} = 346.6\,\text{Pa} \tag{17b}$$

0.1.7.3 Uncertainty in Compressed Pressure

The bias uncertainty in the compressed pressure is due to the standard error in the piezoelectric pressure transducer. According to the manufacturer's calibration, the deviation of the full scale output from linearity is less then 0.2%, indicating that $B_{T_C} = 0.5\,\text{bar}$. The uncertainties in the signal acquisition equipment are negligible compared to this uncertainty. The precision uncertainty is due to the limit of precision of the output of the pressure, and is $5 \times 10^{-7}\,\text{bar}$. This is negligible compared to the bias uncertainty, so the total uncertainty of the compressed pressure is

$$U_{P_C} = B_{T_C} = 0.5\,\text{bar} \tag{18}$$

0.1.7.4 Uncertainty in the Specific Heat

The uncertainty in the specific heat comes from two sources. First is the uncertainty in the mixture composition and second is the uncertainty in the linear fit to the total specific heat. The uncertainty in the mixture composition can be estimated by the same method as is used for T_C. The specific heat is given by Eq. (8), so we can take partial derivatives of that equation with respect to the mole fractions of the species to find the total uncertainty

$$
\begin{aligned}
\left(U_{\hat{C}_{p,\text{total}}}\right)^2 &= \left(\frac{\partial \hat{C}_p}{\partial X_1} U_{X_1}\right)^2 + \ldots + \left(\frac{\partial \hat{C}_p}{\partial X_n} U_{X_n}\right)^2 \\
&= \left(\hat{C}_{p,1} U_{X_1}\right)^2 + \ldots + \left(\hat{C}_{p,n} U_{X_n}\right)^2
\end{aligned}
\tag{19}
$$

where n is the total number of species. In Eq. (19), it is assumed that the uncertainty in the specific heats of each species is negligible. This is considered an acceptable assumption for stable species such as the fuel molecules, oxygen, nitrogen, and argon. Experience with several kinetic mechanisms has shown that the typical variation in individual $\hat{C}_p$ fits causes approximately 1 K changes in T_C.

The uncertainty of the mole fraction of the species is estimated differently depending on how

Table 1: Mixtures studied in the uncertainty analysis.

Fuel	Mole Fraction			
	Fuel	Oxygen	Nitrogen	Ar
Methylcyclohexane	0.0107	0.2240	0.0000	0.7653
n-Butanol	0.0676	0.2030	0.7294	0.0000
i-Pentanol	0.0531	0.1989	0.7480	0.0000
Propene	0.0854	0.1921	0.7225	0.0000

the species was introduced to the mixing tank. For liquid fuel species, experiments with GC/MS have shown that there is approximately 5% variation in mole fraction from the expected value [20]; this value is adopted for the total uncertainty of all liquid fuels. The mole fraction of the gaseous species is determined by their partial pressures when filling; the mole fraction is related to the pressure by Dalton's Law of Partial Pressure [27, 28]

$$X_i = \frac{P_i}{P} \tag{20}$$

where P_i is the partial pressure of a species and P is the total pressure. It follows that

$$
\begin{aligned}
\left(U_{X_i}\right)^2 &= \left(\frac{\partial X_i}{\partial P_i} U_{P_i}\right)^2 + \left(\frac{\partial X_i}{\partial P} U_P\right)^2 \\
&= \left(\frac{U_{P_i}}{P}\right)^2 + \left(\frac{-P_i}{P^2} U_P\right)^2
\end{aligned}
\tag{21}
$$

The uncertainties of the pressures P_i and P are equal and can be estimated by the same procedure as in Sec. 0.1.7.2 since the same pressure transducer is used to measure the pressure. The total pressure P will be different for each species as it is filled. The order followed in these experiments is liquid fuel injection, followed by oxygen, then nitrogen, then argon.

A typical total pressure after filling is approximately 1300 Torr ($\approx$ 173,319 Pa). The mixtures in Table 1 are the mixtures that will be analyzed in the following because they represent a worst case scenario in that the mole fraction of the fuel or oxygen is maximized in them.

Once the total specific heat has been calculated, a linear fit as a function of temperature is

applied by least-squares estimation. Since there is an uncertainty in the specific heat, there is a corresponding uncertainty in the fit coefficients a and b. Following the methodology outlined by York et al. [29], the values and uncertainties of a and b are calculated iteratively. This procedure gives identical values of the slope, intercept, and standard errors as maximum likelihood estimation [29]. Equation (22) is reproduced from York et al. [29], and is presented as Eq. (13) in that work.

$$a = \overline{Y} - b\overline{X} \tag{22a}$$

$$b = \frac{\sum W_i \beta_i V_i}{\sum W_i \beta_i U_i} \tag{22b}$$

$$\sigma_a^2 = \frac{1}{\sum W_i} + \overline{x}^2 \sigma_b^2 \tag{22c}$$

$$\sigma_b^2 = \frac{1}{\sum W_i u_i^2} \tag{22d}$$

where the symbols in Eq. (22) are defined in Table 2. The general formulation is given here because it will be reused in **??**; application to this section will be given below.

In this section, X_i are the temperatures at which Eq. (10) is evaluated and Y_i are the total specific heats evaluated from Eq. (10). The weighting of the specific heats—$\omega(Y_i)$—is taken to be the reciprocal of the uncertainty as calculated by Eq. (19). Furthermore, there is no uncertainty in the abscissa (i.e. the temperature) and $\omega(X_i) = 1$. Finally, since there is no uncertainty in the temperature, there is no correlation between the uncertainties, i.e. $r_i = 0$.

First, the slope b is estimated by simple least-squares regression of the total specific heat on the temperature. Then, this slope is used to estimate the adjusted weighting of each point, W_i. Next, U_i and V_i are calculated based on the adjusted weighting. Using U_i, V_i, and β_i, a new value of the slope is calculated from Eq. (22b), and the process is repeated until the slope converges. Convergence is determined when the slope changes by less than 0.001 on successive iterations. Then, using Eq. (22a), the intercept a is calculated. Finally, the standard error of each parameter is calculated using the final values of the slope and intercept with Eqs. (22c) and (22d)).

For the mixtures considered in this study, the correlation coefficient for the linear fits are greater than 0.99 (i.e. $r^2 > 0.99$), indicating a good fit.

Table 2: Symbols in Eq. (22). Reproduced from the work of York et al. [29].

Symbol	Meaning
a, b	y intercept and slope of best line, $y = a + bx$
σ_a, σ_b	Standard errors of a and b
X_i, Y_i	"Observed" data points
r_i	Correlation coefficient between uncertainty in X_i and Y_i
$\omega(X_i), \omega(Y_i)$	Weights of X_i and Y_i
x_i, y_i	Least squares adjusted points: $\overline{X} + \beta_i, \overline{Y} + b\beta_i$
α_i	$\sqrt{\omega(X_i)\omega(Y_i)}$
W_i	$\dfrac{\omega(X_i)\omega(Y_i)}{\omega(X_i) + b^2\omega(Y_i) - 2r_i\alpha_i b}$
$\overline{X}, \overline{Y}$	$\dfrac{\sum W_i X_i}{\sum W_i}, \dfrac{\sum W_i Y_i}{\sum W_i}$
U_i, V_i	$X_i - \overline{X}, Y_i - \overline{Y}$
$\overline{x}$	$\dfrac{\sum W_i x_i}{\sum W_i}$
β_i	$W_i\left[\dfrac{U_i}{\omega(Y_i)} + \dfrac{bV_i}{\omega(X_i)} - (bU_i + V_i)\dfrac{r_i}{\alpha_i}\right]$
u_i	$x_i - \overline{x}$

0.2 Fast Sampling System

The fast sampling system (FSS) used in this work is a commercial system supplied by SME-Tec Gmbh. from Germany. The FSS is composed of two parts, the gas sampling valve (GSV) and the Controller. A schematic of the GSV is shown in **??**. Gases are admitted from the reaction chamber into the heated carrying tubes through the poppet-style valve on the left of the GSV. The sampled gases are then conducted through the GSV outlet into the 150 mL sampling bottle.

A schematic of the GSV assembly is shown in **??**. The GSV is mounted to the RCM by a custom-made end plug. The reaction chamber is sealed by an O-ring on the small- and large-diameter portions of the GSV. The depth that the GSV is inserted into the reaction chamber is adjustable by adding or removing shims in the end plug assembly. The insertion depth is chosen so that the tip of the GSV is outside the boundary layer on the end wall.

The portion of the GSV protruding into the reaction chamber has minimal effect on the homogeneity of the reaction chamber. Moreover, the removal of samples also has minimal effect on the measured ignition delay. This has been verified experimentally by measuring the ignition delay with and without the GSV present, and with and without sampling occurring. In both cases, the difference in ignition delay was statistically insignificant for $\alpha = 0.05$.

The close-open-close (COC) cycle of the GSV is controlled by a mass-spring system. The poppet face is connected to a rod running the length of the GSV and connected to the mass at the rear of the valve. To open the poppet, the mass is accelerated forward by passing current through the coil around the mass. The rod is also connected to a spring that is used to restore the poppet to its original position after being extended.

The GSV has an adjustable COC time, by adjusting the distance the plate is allowed to move. Furthermore, the GSV has the ability measure the displacement of the mass, allowing the direct measurement of the COC time and the absolute time of opening.

The GSV controller is triggered by a 5 V signal from the cDAQ. The timing of the trigger signal is controlled by the LabView VI. The pressure signal from the reaction chamber is read

from the cDAQ in 1 ms chunks in a loop. On each loop iteration, the maximum pressure is checked against a desired trigger pressure; when the reaction chamber pressure exceeds the trigger pressure, the cDAQ sends the trigger to the GSV controller. The GSV controller has an adjustable delay (4.5–50 ms) that is used to control the timing of the opening of the GSV during the induction period. The absolute opening time of the GSV is thus dependent on three parameters:

1. The cable delays from the PC to the cDAQ; from the cDAQ to the GSV controller; and from the GSV controller to the GSV itself

2. The processing time of the LabView VI

3. The delay set in the GSV controller.

However, since the absolute opening time of the GSV can be measured by the signal sent from the GSV to the controller (and thence to the cDAQ), the uncertainty in the opening time is actually quite small, and is related to the cable delay in sending the COC signal from the GSV to the cDAQ and the precision of the A/D conversion in the cDAQ. The uncertainty of the absolute opening time is thus estimated as $\pm 1\,\mu$s.

Furthermore, the correspondence of the COC signal from the valve with the physical valve movements has been experimentally verified by high speed video. Frames from these videos are shown in **??**. The frames show that the opening and closing times of the valve face correspond closely with repeatable points in the peak of the voltage.

Missing figure   GSV Video

0.2.1 Experimental Procedure

Prior to an experiment, the GSV and sampling bottle are vacuumed to less than 1 Torr. The reaction chamber is vacuumed and filled in the same procedure as described previously, and the compression is triggered. For a given trigger pressure and controller delay, the GSV opens at some time after the EOC and removes a gas sample from the reaction chamber. The sample is diluted by high purity helium. Then the sample bottle is disconnected from the GSV and transported to the Gas Chromatograph/Mass Spectrometer, where the sample undergoes analysis.

0.3 Gas Chromatograph/Mass Spectrometer

0.3.1 Theory of Gas Chromatography/Mass Spectrometry

0.3.1.1 Gas Chromatography

A gas chromatograph (GC) is a device that physically separates components of a gas sample by means of a tube—known as a *column*—lined or filled with a substance that interacts with the components in the sample. The sample is transported the length of the column by a flow of carrier gas, usually helium or hydrogen, also known as the *mobile phase*. A detector is placed at the outlet of the column to measure the amount and type of components eluted from the column.

The separation of the gaseous components in the sample is effected by the interaction of the sample with the lining of the column, known as the *stationary phase*. Gaseous species that have little interaction with the stationary phase and spend most of their time in the mobile phase are eluted from the column before species that interact strongly with the stationary phase and spend little time in the mobile phase [30].

The column is placed in an insulated oven so that its temperature may be controlled. The column temperature in a given analysis may be constant or may be controlled as a function of time. Since the time that a given component takes to move through the column is a function of temperature,

this facility allows optimization of the elution time of the various components in the sample.

The injector of the GC is also temperature controlled; the temperature of the injector is set high enough so that all components (including the solvent, if any) are vaporized but not so high that the sample starts to degrade. On the present GC, a split/splitless injector is installed. This allows for operation in the split mode, where a percentage of the injected sample is removed from the injector prior to injection onto the column, or in the splitless mode, where nearly all of the sample is injected into the column. The split mode is used in this work. The amount of sample removed is controlled by a valve in the injector. The split ratio is calculated according to Eq. (23)

$$\text{Split Ratio} = \frac{\text{Column Flow} + \text{Vent Flow}}{\text{Column Flow}} \tag{23}$$

where the column flow is the carrier gas flow rate at the head of the column and the vent flow is the flow out of the splitter vent [30].

A GC may also be equipped with a gas sample injection valve, in addition to the split/splitless injector. This valve is connected serially prior to the split/splitless injector. The present GC is equipped with a 10-port Valco sample injection valve, shown schematically in Fig. 5. Each port is numbered, and curved lines indicate connections between ports. The sample injection valve is used to inject a consistent mass of sample into the column with each injection. This permits reliable quantification of the components in the sample. First, the sample is loaded into the sample loop when the valve is in the "load" position, as in Fig. 5a. Then, the valve is electrically actuated at the start of the GC run to rotate the connections into the "inject" position. This allows carrier gas to flow through the sample loop and push the sample from the sample loop into the column via the split/splitless injector (Fig. 5b). The valve is then actuated again to remove the sample loop from the carrier gas path and restore the "load" position (Fig. 5a).

The sample injection valve is equipped with a heater to maintain the valve body at a constant temperature and the entire assembly is installed in an insulated box. However, this heater is insufficient to heat the tubes attached to the valve, so an additional heater rope is installed in the insulated
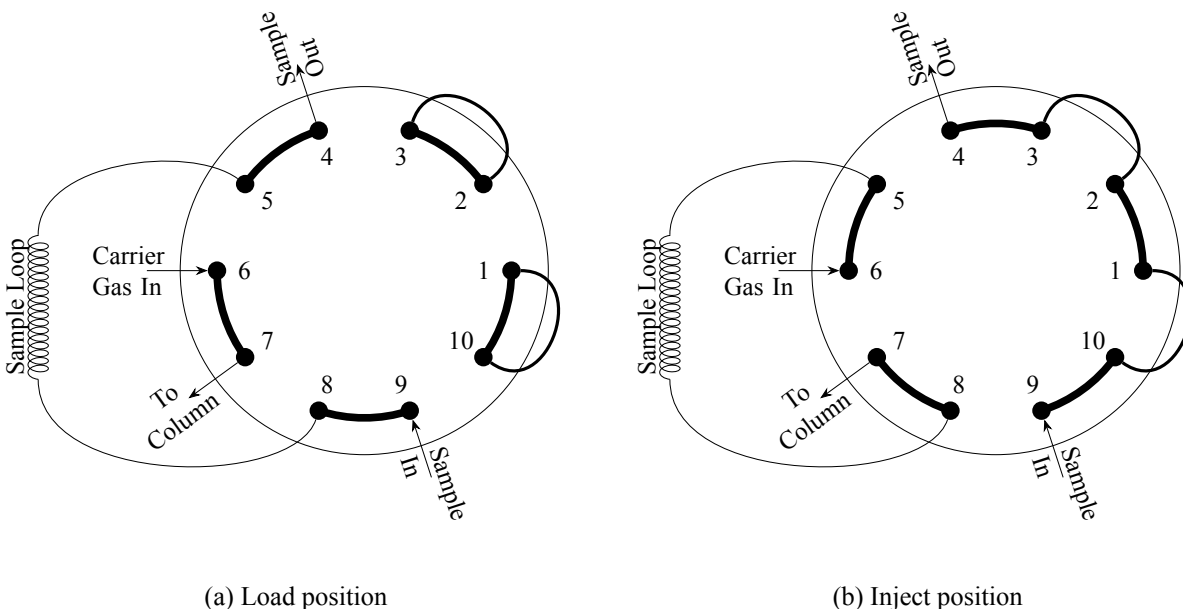
(a) Load position   (b) Inject position

Figure 5: GC/MS sample injection valve.

box. To measure the temperature of the sample loop directly, a thermocouple is fixed to the sample loop by ceramic cement. The temperature of the sample loop is used to control the power provided to the rope heater, while a built-in thermocouple is used to control the power provided to the valve body heater, so that the sample loop remains at a constant temperature.

0.3.1.2   Mass Spectrometry

Many types of detectors are available for GC analyses. These commonly include flame ionization detectors, thermal conductivity detectors, and mass spectrometers. In this work, a mass spectrometer is used to identify and quantify the species eluted from the column.

The fundamental operation of a mass spectrometer (MS) is to detect the spectrum of ions in a given sample. The MS generates this spectrum by detecting the mass-to-charge (m/z) ratios of the ions. Ions are generated from the effluent of the column—which includes sample components, mobile phase, and column bleed, collectively called *analytes*—by an ionization source, typically either electronic or chemical in nature. Nearly all of the ions generated will have a single charge, $z = 1$ [31]; thus, the m/z value of the ions is also equal to the mass of the ion.
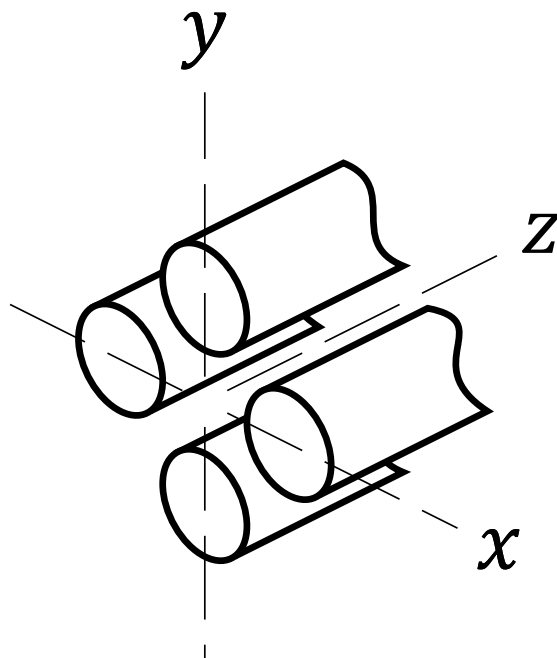
Figure 6: Schematic of the transmission quadrupole in an MS.

In this work, electron ionization (EI) is used to generate the ions for analysis. The effluent from the column is passed in front of an electron source so that the electrons impact the analyte molecules and remove an electron, generating a positive ion. EI is a *hard ionization* technique, in that the electron impact transfers a significant amount of energy to the analyte molecule [31]. The additional energy causes the ion to fragment into two or more pieces; the spectrum of these fragments is characteristic for a given molecule and can be used as a "fingerprint" to identify the source molecule for a given spectrum.

After ionization, the fragments are formed into a beam and accelerated out of the ionization chamber towards the detector. Several detectors are available, including time-of-flight and transmission quadrupole. All of these detectors require high vacuum to avoid impact of the ion beam with extraneous species prior to reaching the detector. The vacuum is achieved in the present MS by a two-stage design, using a rotary vane pump in series with a turbomolecular pump to achieve ultimate pressures of approximately 2 Pa.

The MS used in this study is a transmission quadrupole type, shown schematically in Fig. 6. The transmission quadrupole separates specific ions from the ion beam by means of a time-varying

electric field. Conceptually, the quadrupole can be imagined as four round rods, arranged in a cross pattern, with their long axes aligned parallel to the ion beam (i.e. the z axis). The ions are admitted to the rods at one end (e.g. at the origin in Fig. 6) and the detector is placed parallel to the $x - y$ plane in Fig. 6 at the other end of the rods(not shown in Fig. 6). A positive DC voltage is applied to one pair of the rods, while a negative DC voltage is applied to the other pair of rods; in addition, an AC voltage is applied simultaneously to all four rods. Assuming a specific ratio of AC amplitude to DC amplitude, ions of a certain m/z will remain in the ion beam and reach the detector. Then, holding the AD:DC amplitude ratio fixed, the amplitudes are ramped with a known function of time. This varies the particular m/z that will remain in the ion beam and reach the detector to be recorded [31], generating a mass spectrum.

The voltage amplitudes are ramped many times per second—typical ramp times range from 0.05–0.5 s, depending on the range of m/z values to be acquired—so that many spectra are acquired during the elution of a given chemical compound from the column, which typically occurs on the order of a few seconds. For a given scan from the lowest to the highest amplitude, the number of ions of each m/z is measured at the detector. This information is typically presented in the form of a relative intensity plot. The abscissa is the (integer) m/z while the ordinate is the intensity of a particular m/z scaled by the maximum intensity of all the m/z in a given scan. It is not required that the m/z be integers, although they are usually presented as such for simplicity. An example of a mass spectrum for a given time in a GC/MS analysis is shown in Fig. 7.

In addition to the mass spectrum, the MS reports the total ion current (TIC), also known as the total ion chromatogram. This is the sum of all of the mass intensities for a given scan. A sample TIC is plotted in Fig. 8 where the abscissa is time in min and the ordinate is an arbitrary unit. Finally, the MS can also report the mass chromatogram (MC), which is the chromatogram for a specific m/z as a function of time.
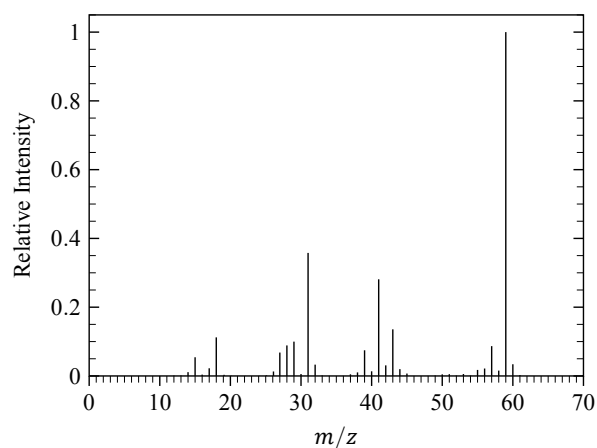
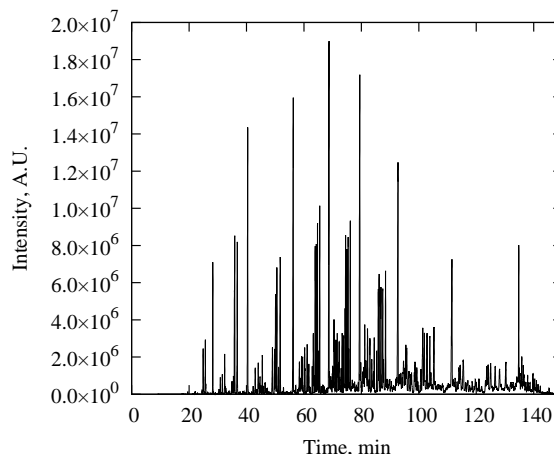**Figure 7**: Example mass spectrum for a given scan during a GC/MS analysis

Figure 8: Example TIC for a GC/MS analysis

0.3.2 Identification and Quantification of Species using GC/MS

Species are identified using a GC/MS system by their unique mass spectra. Each peak in the TIC typically represents one compound eluting from the column, although in theory each peak can represent more than one compound if the compounds are retained similarly by the column. The peak is caused by an increase in the number of ions reaching the detector on each scan relative to the baseline as the compound elutes and is ionized. As mentioned previously, many scans of the desired m/z range are conducted over the time that a compound is eluting from the column. To determine the identity of a compound in a given peak, the set of mass intensities over the peak are averaged and the background spectrum is subtracted; this average spectrum is compared to a database supplied by the National Institute of Standards and Technologies (NIST). The database returns several suggested species with a degree of matching parameter indicating how well the supplied spectrum matches the spectrum in the database.

In this work, the external standard method of quantification is used. This requires that calibration curves for each of the species of interest be created, relating the area of the peak in the TIC to the number of moles of analyte reaching the detector. The number of moles of analyte can in turn be related to the number of moles of sample in the gas sample injection valve sample loop. Once the calibration curve is generated, it is used to relate the measured area of the peak of particular

28

component to its mole fraction. Detailed methods for the construction of calibration curves will be given in Sec. 0.3.3.

0.3.3 Experimental Procedure

The GC/MS used in this study is a Shimadzu model QP-2010S, equipped with a 10-port Valco sample injection valve and split/splitless injector, as mentioned previously. The column used is a Phenomenex model ZB-5MS capillary column with length 30 m, inner diameter 0.25 μm, and film thickness of 0.25 μm. The operating parameters of the GC/MS (known as the "method") are shown in **??**.

The pressure in the gas injection valve sample loop is monitored by an MMA type pressure transducer, the same model as used in Sec. 0.1.7.2. The sample outlet in Fig. 5 is open to the atmosphere so that a consistent pressure is maintained in the sample loop. The volume of the sample loop is 10 μL. With the temperature, pressure, and volume of the sample loop known, the number of moles of sample can be calculated by the ideal gas law.

A calibration curve is built for the major species by the following procedure. First, the sample bottle is vacuumed to less than 1 Torr. Mixtures of the species of interest in the liquid state are prepared by massing each component on a high-accuracy AND-201 scale. A small mass of this mixture is drawn into a syringe and massed on the same scale. The mixture is injected through a septum into the sample bottle. Then the sample bottle is filled with high-purity nitrogen so that the largest mole fraction of a species of interest is approximately 0.001. The sample bottle is connected to the sample injection valve on the GC/MS and the valve on the sample bottle is opened and quickly closed. The pressure is allowed to equalize and the GC/MS is started.

After the completion of the GC/MS method, the total ion chromatogram (TIC) is analyzed by the Shimadzu GCMS Post-run Analysis software (version XXXX). Each peak is automatically integrated by the software so that its area can be found. The peak area is then related to the number of moles of sample sent to the detector by linear least-squares regression. This calibration curve is used to compute the mole fraction of any given peak area for that species.